

Electron-photon Chern number in cavity-embedded 2D moiré materials

Danh-Phuong Nguyen,¹ Geva Arwas,¹ Zuzhang Lin,^{2,3} Wang Yao,^{2,3} and Cristiano Ciuti¹

¹*Université Paris Cité, CNRS, Matériaux et Phénomènes Quantiques, 75013 Paris, France*

²*Department of Physics, The University of Hong Kong, Hong Kong, China*

³*HKU-UCAS Joint Institute of Theoretical and Computational Physics at Hong Kong, China*

(Dated: September 27, 2023)

We explore theoretically how the topological properties of 2D materials can be manipulated by cavity quantum electromagnetic fields for both resonant and off-resonant electron-photon coupling, with a focus on van der Waals moiré superlattices. We investigate an electron-photon topological Chern number for the cavity-dressed energy minibands that is well defined for any degree of hybridization of the electron and photon states. While an off-resonant cavity mode can renormalize electronic topological phases that exist without cavity coupling, we show that when the cavity mode is resonant to electronic miniband transitions, new and higher electron-photon Chern numbers can emerge.

In recent years van der Waals heterostructures combining atomic-thin layers of 2D materials such as graphene or transition metal dichalcogenides (TMD) have attracted a great deal of interest [1–6]. Indeed, these systems present rich and controllable physical properties already at the single-particle level due to multiple quantum degrees of freedom, namely the electron spin, the valley and layer pseudospins. This class of 2D materials exhibits a wide variety of interesting electronic properties including semimetallic, semiconducting, superconducting and magnetic phases. One prominent example is magic angle twisted bilayer graphene, exhibiting quasi-flat electronic bands [7] and remarkable superconducting properties [8]. Another notable class of moiré heterostructures is based on TMD materials, which, thanks to their semiconductor properties, have particularly interesting optical properties [9–11].

A growing interest is emerging for the manipulation of materials with cavity vacuum fields [12–15]. In particular, metallic split-ring terahertz electromagnetic resonators are remarkable for their deeply sub-wavelength photon mode confinement [16–18] with mode volumes that can be as small as $10^{-10}\lambda_0^3$, being λ_0 the free-space electromagnetic wavelength corresponding to the resonator frequency. Studies on GaAs 2D electron gases have shown that electronic transport in mesoscopic quantum Hall bars can be greatly modified by the coupling to electromagnetic resonators even without illumination [19], as a result of cavity-mediated electron hopping [20, 21], which results in a breakdown of the Hall resistance quantization associated to the topological properties of the electronic Landau states.

Recent theoretical works have investigated how to exploit cavity QED to control topological properties of systems, such as 1D tight-binding chains described by the SSH model [22]. Concerning 2D systems, a recent work has studied 2D bulk materials [23, 24] where the standard electron Chern number is computed by considering an effective electronic Hamiltonian obtained by adiabatic

elimination of the photon degrees of freedom. A letter exploring single-sheet graphene ribbons [25] has studied electron Chern numbers computed once the cavity field is approximated in a classical coherent state. Another investigation has explored a generic single-electron problem in the ultrastrong light-matter coupling regime [26] and focused on the topological control in the configuration where the cavity photon mode frequency is much larger than the relevant electronic transition frequencies. A key point that has not been addressed is the behavior of genuine electron-photon topological invariants that are associated to the interacting quantum electron-photon system when the photon mode is resonant to electronic transitions. In the past, this has been done only for classical exciton-polariton normal modes where a bosonic exciton field is strongly coupled to a cavity photon field [27, 28] (the bare cavity photon and exciton bands are topologically trivial, but the hybrid light-matter polariton bands are not). However, for a fermionic particle coupled to a quantized cavity field, to the best of our knowledge, the study of electron-photon topological invariants for the resonant light-matter coupling has been overlooked.

In this letter, we explore the properties of electron-photon Chern numbers, focusing on cavity-embedded 2D moiré materials. We investigate different regimes of coupling (off-resonant versus resonant cavity mode), for different cavity geometries (mode with in-plane or out-of-plane polarization) and explore the topological transitions characterized by such an electron-photon Chern number with realistic values for state-of-the-art split-ring resonators and TMD materials. We show that in the case of resonant electron-photon coupling, new topological phases and high Chern numbers can emerge.

Cavity QED Hamiltonian — Let us consider a bilayer moiré system consisting of two twisted TMD layers embedded in a single-mode resonator (see the sketch in Fig. 1). Each of them is a honeycomb lattice defined by two primitive translation vectors $\mathbf{a}_1 = a_0\sqrt{3}/2(1, \sqrt{3}, 0)$ and $\mathbf{a}_2 = a_0\sqrt{3}/2(-1, \sqrt{3}, 0)$, where a_0 is the monolayer TMD

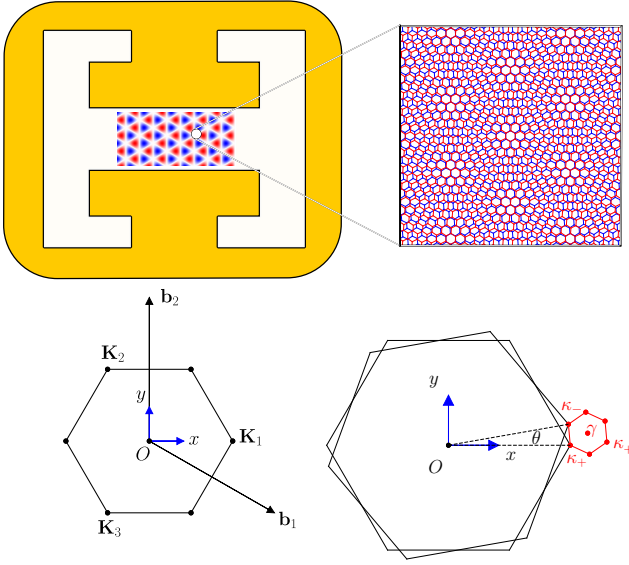


FIG. 1. Top panel: sketch of a twisted bilayer system with its moiré pattern inside the gap region of a split-ring resonator. Bottom panel: on the left, the first Brillouin zone with Dirac points of the bottom layer and corresponding wavevectors; on the right, the Brillouin zones of both the bottom and rotated top layer together with the moiré mini Brillouin zone (shown in red) for the corresponding moiré superlattice.

lattice constant. We consider in-plane parallel stacking (R-stacking) with the layer on top rotated by a small angle θ in order to create a long wavelength moiré pattern. The distance between two layers is d . The moiré unit cell is defined by $\mathbf{L}_{i=1,2} = [\mathbb{1} - R(\theta)^{-1}]^{-1} \mathbf{a}_i$, where $\mathbb{1}$ and $R(\theta)$ are respectively the identity and the rotation matrix corresponding to the rotation angle θ about the z -axis. We denote the moiré lattice constant $|\mathbf{L}_i|$ as a_M , where for small angles $a_M \simeq a_0/\theta$. In the following, for numerical applications we will use parameters of the MoTe₂ system [29]. For the photonic part, thanks to the approximately flat mode inside the capacitive gap of complementary split-ring resonators [19], we will consider a single-mode cavity with a spatially homogeneous field described by the vector potential $\hat{\mathbf{A}} = A_0 \mathbf{u}(\hat{a} + \hat{a}^\dagger)$ with \hat{a}^\dagger (\hat{a}) the photonic creation (annihilation) operator.

The vacuum field amplitude is $A_0 = \sqrt{\hbar/(2\omega_c\epsilon_0 V_{mode})}$ with ω_c the mode frequency, $V_{mode} = \eta\lambda_c^3$ the effective mode volume related to the compression factor η and λ_c the wavelength in free space that corresponds to ω_c . The orientation of the cavity mode polarization is described by the unit vector $\mathbf{u} = (u_x, u_y, u_z)$.

Our treatment is based on the four-band continuum model for small angle twisted bilayer TMD [29, 30]. The cavity QED Hamiltonian can be written as

$$\hat{H} = \hbar\omega_c\hat{a}^\dagger\hat{a} + \begin{pmatrix} \hat{H}_t & 0 \\ 0 & \hat{H}_b \end{pmatrix} + \begin{pmatrix} \hat{V}_t & \hat{U} \\ \hat{U}^\dagger & \hat{V}_b \end{pmatrix}, \quad (1)$$

where the 2×2 operator matrix \hat{H}_t (\hat{H}_b) corresponds to the conduction and valence bands of the top (bottom) layer. The moiré potentials are given by the last term. The light-matter coupling is introduced via Peierls factors [31] in the intralayer (\hat{H}_t , \hat{H}_b) and interlayer (\hat{U}) hopping terms. We quantify the interaction strength by the dimensionless constant $g = eA_0a_0/\hbar$. For $g \ll 1$ and in the low-energy sector, each diagonal block matrix $\nu = t, b$ and interlayer coupling \hat{U} can be approximated as follows:

$$\begin{aligned} \hat{H}_\nu &= \Delta\sigma_z + v_F\boldsymbol{\sigma}_{xy} \cdot [\hat{\mathbf{p}} - \hbar\mathbf{K}_\nu + e\mathbf{A}^{(xy)}(\hat{a} + \hat{a}^\dagger)], \\ \hat{U} &= e^{-i\frac{eA^{(z)}d}{\hbar}(\hat{a} + \hat{a}^\dagger)}\hat{U}_0, \end{aligned} \quad (2)$$

with $\mathbf{K}_t = \boldsymbol{\kappa}_-$, $\mathbf{K}_b = \boldsymbol{\kappa}_+$ shown in Fig. 1, $\boldsymbol{\sigma}_{xy} = (\sigma_x, \sigma_y, 0)$ a vector of Pauli matrices, $\mathbf{A}^{(xy)}$ is the in-plane projection of $A_0\mathbf{u}$ and $A^{(z)}$ is its z -component. Note that the interlayer distance d is much larger than the in-plane lattice constant a_0 . Hence, the argument of the Peierl's exponential for the U term is much larger than its t counterpart (in-plane coupling). We will consider a regime of realistic parameters, where it turns out that the exponential of the t -term can be linearized, while the out-of-plane Peierls term must be kept in exponential form. The moiré potentials \hat{V}_ν and \hat{U}_0 are the same as the ones in [29, 30]. Due to the large energy gap between the conduction and valence band in the TMD material, we can restrict our description to the latter, for which non-trivial topological properties were studied [29, 32] in the absence of a cavity field. Finally, we represent the Hamiltonian in the hole picture. The corresponding Hamiltonian reads:

$$\hat{H} = \hbar\omega_c\hat{a}^\dagger\hat{a} + \frac{1}{2m^*} \begin{pmatrix} (\hat{\mathbf{p}} + \hbar\boldsymbol{\kappa}_- - e\mathbf{A}^{(xy)}(\hat{a} + \hat{a}^\dagger))^2 & 0 \\ 0 & (\hat{\mathbf{p}} + \hbar\boldsymbol{\kappa}_+ - e\mathbf{A}^{(xy)}(\hat{a} + \hat{a}^\dagger))^2 \end{pmatrix} - \begin{pmatrix} \hat{V}_t^v & \hat{U}_0^{v\dagger} \\ \hat{U}_0^v & \hat{V}_b^v \end{pmatrix} - i\frac{\omega_c e A^{(z)} d}{2}(\hat{a} - \hat{a}^\dagger)\tau_z \quad (3)$$

where $m^* = \Delta/v_F^2$ is the effective mass of the valence band, τ_z is the z -axis Pauli matrix with respect to the layer pseudospin. We have considered minimal coupling in the Coulomb gauge for the in-plane motion, while

the dipole gauge resulting from a Power-Zienau-Woolley (PZW) transformation is used for the out-of-plane part. The expression for the moiré potentials \hat{V}_t^v , \hat{V}_b^v , \hat{U}_0^v is the same as in [29, 30] and is reported in the Supple-

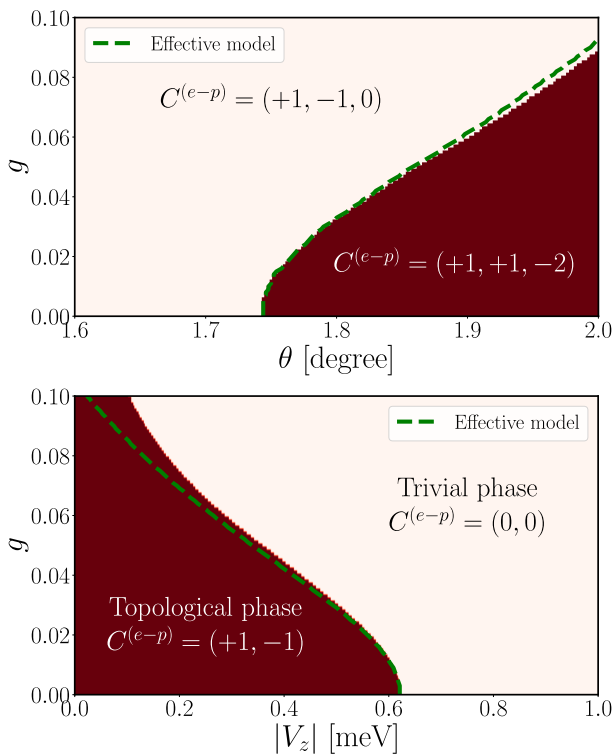


FIG. 2. Electron-photon Chern numbers of the first three (top panel) and two (bottom panel) moiré minibands of the twisted TMD bilayer system (MoTe₂ parameters). The dashed lines depict the phase boundary predicted by an effective electronic Hamiltonian obtained by adiabatically eliminating the photonic degrees of freedom [21] and calculating the electron Chern number. Top panel: Chern numbers versus the twisting angle θ and the dimensionless cavity coupling g (see definition in the text), with no inter-layer bias ($V_z = 0$). Bottom panel: Chern numbers versus V_z and the dimensionless cavity coupling g for a fixed angle $\theta = 1.2^\circ$. Parameters: cavity photon energy $\hbar\omega_c = 20$ meV (top panel) and 6 meV (bottom panel), cavity mode polarization vector $\mathbf{u} = (1, 0, 0)$.

mental Material. To account for the interlayer bias V_z (that breaks the symmetry between κ_+ and κ_- [29]), the term $-V_z/2 \times \tau_z$ has to be added to the Hamiltonian in Eq. (3). As the moiré potential is periodic with respect to $\mathbf{L}_{i=1,2}$ translations, the electronic part can be block-diagonalized in momentum space (Bloch theorem). Each block \mathbf{k} belongs to the moiré mini Brillouin zone (mBZ) shown in Fig. 1, spanned by moiré reciprocal vectors \mathbf{G}_1 and \mathbf{G}_2 satisfying $\mathbf{G}_i \cdot \mathbf{L}_j = 2\pi\delta_{ij}$.

Definition of the electron-photon Chern number — Let us consider a single fermion interacting with a cavity quantized field. This is equivalent to injecting a fermion into empty minibands. If the fermion wavevector \mathbf{k} is a good quantum number, then we can diagonalize the Hamiltonian $\hat{H}_{\mathbf{k}} = e^{-i\mathbf{k}\cdot\hat{\mathbf{r}}}\hat{H}e^{i\mathbf{k}\cdot\hat{\mathbf{r}}}$ and obtain electron-photon eigenstates of the form $|\Psi_{n\mathbf{k}}^{(e-p)}\rangle$ with corresponding electron-photon energy bands $\mathcal{E}_{n\mathbf{k}}^{(e-p)}$. Given the form of the system eigenstates, we can introduce the following

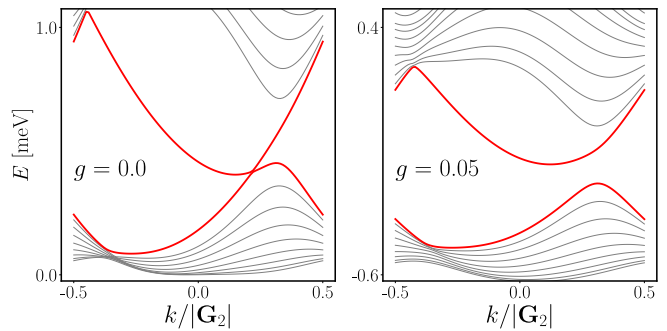


FIG. 3. Electron-photon energy-momentum dispersions $\mathcal{E}_{n\mathbf{k}}^{(e-p)}$ for $g = 0.0$ (left panel) and 0.05 (right panel) for a ribbon geometry (periodic boundary conditions along the long direction). Parameters: cavity photon energy $\hbar\omega_c = 6$ meV, $V_z = 0.5$ meV, $\theta = 1.2^\circ$, ribbon width $D_1/a_M = 10$ and cavity mode polarization vector $\mathbf{u} = (1, 0, 0)$. Here, the photonic component of the electron-photon eigenstates is small (see text).

electron-photon Chern number:

$$\mathcal{C}_n^{(e-p)} = \int \frac{d^2k}{2\pi} i \sum_{\mu,\nu} \epsilon_{\mu\nu} \langle \partial_{k_\mu} \Psi_{n\mathbf{k}}^{(e-p)} | \partial_{k_\nu} \Psi_{n\mathbf{k}}^{(e-p)} \rangle, \quad (4)$$

where $\epsilon_{\mu\nu}$ is the two-dimensional Levi-Civita tensor. Importantly, the electron-photon Chern number in Eq. (4) is well defined for any arbitrary hybridization between the single electron and the cavity quantum field. If we work in the hole picture, the particle-hole transformation results in a simple change of sign of such Chern number. Numerically the Chern number in Eq. (4) has been calculated by numerical diagonalization of the Hamiltonian (3) and using the technique reported in Ref. [33].

Results and discussions — In what follows, we use the electron-photon Chern number to investigate topological properties of cavity-embedded moiré systems, focusing on twisted MoTe₂ bilayers. We first consider the scenario of high photon frequency, where the photon is off-resonant with respect to the relevant miniband electronic transitions. In Fig. 2, we report the electron-photon topological Chern numbers associated to the first three moiré minibands of the twisted bilayer TMD system. Here, we consider a cavity mode with in-plane polarization $\mathbf{u} = (1, 0, 0)$. For $g = 0$ (no cavity coupling), the system is known to exhibit a topological transition as a function of the twisting angle θ (top panel) and as a function of the inter-layer bias V_z (bottom panel). In the top panel we consider the case with no bias ($V_z = 0$) for which a topological transition occurs by increasing the twisting angle θ above a critical value ($\approx 1.75^\circ$ at zero g), with Chern numbers changing from $(+1, -1, 0)$ to $(+1, +1, -2)$. The bottom panel corresponds to a situation with a fixed angle $\theta = 1.2^\circ$ for which a transition from topologically nontrivial Chern numbers $(+1, -1, 0)$ to the trivial $(0, 0, 0)$ is achieved when V_z is increased

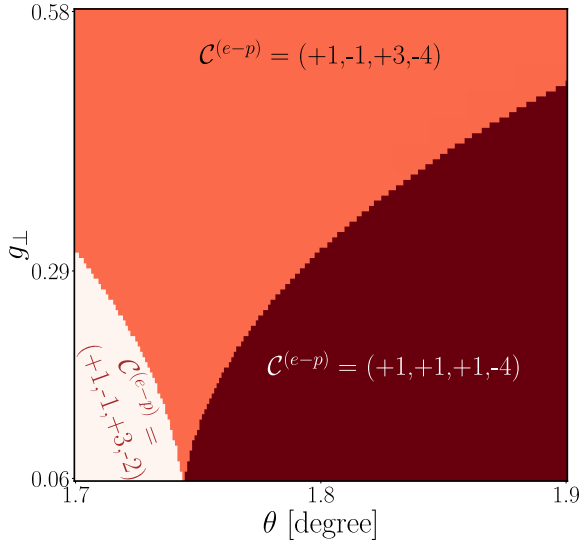


FIG. 4. Electron-photon Chern numbers of the first four moiré minibands for the considered cavity-embedded twisted TMD bilayer system. Note that this topological diagram cannot be predicted by the effective electronic model used in Fig. 2. Other parameters: cavity photon energy $\hbar\omega_c = 10$ meV, $V_z = 0$ meV, and cavity mode polarization $\mathbf{u} = (0, 0, 1)$.

above a critical value (≈ 0.63 meV at zero g). In both situations considered in Fig. 2, a finite cavity coupling modifies the transition boundary significantly for a range of dimensionless coupling g , which is accessible with deeply sub-wavelength resonators. The energy-momentum dispersions with and without the cavity are compared for $V_z = 0.5$ meV in Fig. 3 for a ribbon geometry (periodic boundary conditions along the long direction). The left panel shows the presence of topological edge states that cross in energy for $g = 0$, while the right panel shows the opening of an edge gap in the presence of a cavity with $g = 0.05$. In other words, Fig. 3 shows the consequence of the topological transition with increasing cavity coupling g depicted in the diagram of the bottom panel in Fig. 2.

Note that by tracing out the photonic degrees of freedom, we can obtain an electronic reduced density matrix, namely $\hat{\rho}_{n\mathbf{k}} = \text{Tr}_{\text{phot}}(|\Psi_{n\mathbf{k}}^{(e-p)}\rangle\langle\Psi_{n\mathbf{k}}^{(e-p)}|)$. The electronic purity of such reduced density matrix is defined as $\mathbb{P}_{n\mathbf{k}} = \text{Tr}_{\text{el}}(\hat{\rho}_{n\mathbf{k}}^2)$ [34] and is equal to 1 for a purely electronic state. For $g = 0.1$, the minimum of the electronic purity (the purity depends on \mathbf{k}) is about 75% for the top panel of Fig. 3 and 88% for the bottom one. In such configuration, one might describe the system with an effective electronic Hamiltonian [21–25]. Indeed, we as shown in of Fig. 2 the diagrams are qualitatively reproduced by an effective electronic Hamiltonian approach (see Supplementary Material). However our electron-photon Chern number introduced in Eq. (4) and based on the exact light-matter energies $\mathcal{E}_{n\mathbf{k}}^{(e-p)}$ is defined also for low

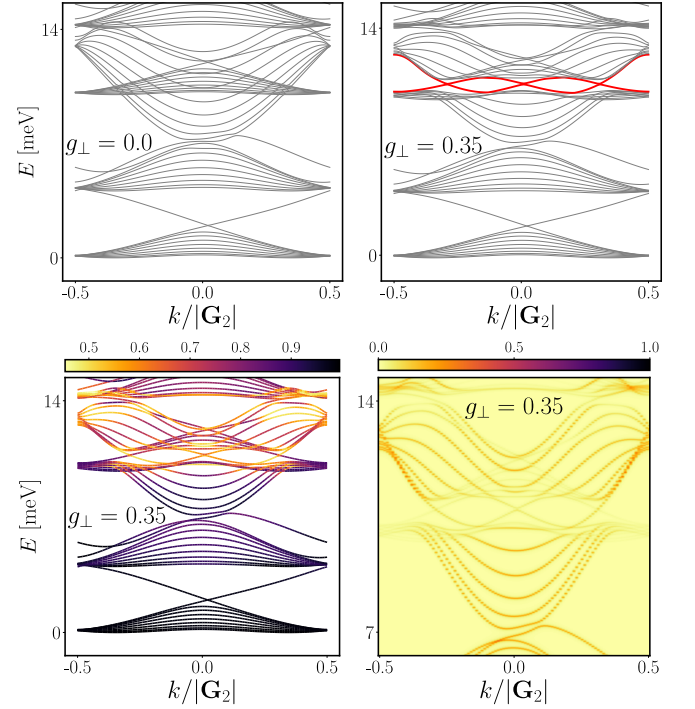


FIG. 5. Top panels: electron-photon miniband dispersions $\mathcal{E}_{n\mathbf{k}}^{(e-p)}$ for $g_{\perp} = 0$ (left panel) and 0.35 (right panel), where three edge states emerge (thicker red lines). Bottom panels: electronic purity (left panel) and electronic spectral function (right panel, normalized by its maximum value) for $g_{\perp} = 0.35$. We have considered a ribbon geometry with width $D_1/a_M = 10$ and periodic boundary conditions along the long direction. Other parameters: cavity photon energy $\hbar\omega_c = 10$ meV, $V_z = 0$ meV, $\theta = 1.8^\circ$, cavity mode polarization $\mathbf{u} = (0, 0, 1)$.

electronic purity, i.e., for any arbitrary light-matter hybridization.

Let us now consider the situation where the cavity mode has a relatively low frequency and is resonant with electronic miniband transitions. Note that we consider here out-of-plane cavity polarization $\mathbf{u} = (0, 0, 1)$ and the corresponding dimensionless coupling constant is defined as $g_{\perp} = eA_0d/\hbar$. The corresponding results are depicted in Fig. 4 and 5. In the non-interacting case ($g_{\perp} = 0$), the photon energy creates replicas of the electronic minibands with non-zero photon numbers, as shown in Fig. 5. The bare electron-photon spectrum becomes degenerate when a photon replica crosses the original electronic miniband with zero photons. However, a finite coupling lifts such degeneracies, leading to new electron-photon energy minibands for which we can compute the electron-photon Chern number. Fig. 4 shows the topological diagram characterized by such an electron-photon Chern number for the first four minibands. The cavity photon energy is resonant to the transition between the first and third electronic minibands, depicted in Fig. 5. The bulk-edge correspondence for the electron-photon Chern number is satisfied: indeed, we observe three edge states shown by

the thicker red line in Fig. 5. These states have low electronic purity (as low as 50%) and cannot be captured by an effective electronic Hamiltonian where the photon degrees of freedom are eliminated. Moreover, such high Chern numbers, created by the hybridization with the cavity photon replicas, are absent in the bare electronic system. These multiple new edge states corresponding to high Chern numbers can be observed by measuring the electronic spectral function via Angle-Resolved Photoemission Spectroscopy (ARPES) [35], Scanning Tunneling Microscopy (STM) [36] or Microwave Impedance Microscopy [37].

Conclusions — In this letter, we explored the new topological phases characterized by the electron-photon Chern number, a topological invariant defined in terms of the exact eigenstates for the Hamiltonian describing a fermionic particle coupled to a quantized electromagnetic field. This is a topological invariant for any arbitrary hybridization of the electron-photon eigenstates. Note that electron-photon Chern numbers can also be defined for disordered and non-homogeneous systems [38–41], so the present topological approach can also be generalized to situations where the cavity mode is not spatially homogeneous or in the presence of electronic disorder. The results of this letter are exact when a single fermion is injected in empty minibands. A future and intriguing problem to explore is how these topological states evolve when such electron-photon states are partially filled.

We acknowledge financial support from the French agency ANR through the project NOMOS (ANR-18-CE24-0026), and TRIANGLE (ANR-20-CE47-0011), CaVdW under the ANR/RGC Joint Research Scheme sponsored by ANR and RGC of Hong Kong SAR China (ANR-21-CE30-0056-01, A-HKU705/21), and from the Israeli Council for Higher Education - VATAT. Z.L. and W.Y. also acknowledge support by RGC of Hong Kong SAR (HKU SRFS2122-7S05, AoE/P-701/20).

-
- [1] A. K. Geim and I. V. Grigorieva, van der Waals heterostructures, *Nature* **499**, 419 (2013).
- [2] P. Ajayan, P. Kim, and K. Banerjee, Two-dimensional van der Waals materials, *Physics Today* **69**, 38 (2016).
- [3] K. S. Novoselov, A. Mishchenko, A. Carvalho, and A. H. C. Neto, 2D materials and van der Waals heterostructures, *Science* **353** (2016).
- [4] J. C. W. Song and N. M. Gabor, Electron quantum metamaterials in van der Waals heterostructures, *Nature Nanotechnology* **13**, 986 (2018).
- [5] O. Ávalos-Ovando, D. Mastrogiuseppe, and S. E. Ulloa, Lateral heterostructures and one-dimensional interfaces in 2D transition metal dichalcogenides, *Journal of Physics: Condensed Matter* **31**, 213001 (2019).
- [6] M. Yankowitz, Q. Ma, P. Jarillo-Herrero, and B. J. LeRoy, van der Waals heterostructures combining graphene and hexagonal boron nitride, *Nature Reviews Physics* **1**, 112 (2019).
- [7] R. Bistritzer and A. H. MacDonald, Moiré bands in twisted double-layer graphene, *Proceedings of the National Academy of Sciences* **108**, 12233 (2011).
- [8] Y. Cao, V. Fatemi, S. Fang, K. Watanabe, T. Taniguchi, E. Kaxiras, and P. Jarillo-Herrero, Unconventional superconductivity in magic-angle graphene superlattices, *Nature* **556**, 43 (2018).
- [9] K. L. Seyler, P. Rivera, H. Yu, N. P. Wilson, E. L. Ray, D. G. Mandrus, J. Yan, W. Yao, and X. Xu, Signatures of moiré-trapped valley excitons in MoSe₂/WSe₂ heterobilayers, *Nature* **567**, 66 (2019).
- [10] K. Tran, G. Moody, F. Wu, X. Lu, J. Choi, K. Kim, A. Rai, D. A. Sanchez, J. Quan, A. Singh, J. Embley, A. Zepeda, M. Campbell, T. Autry, T. Taniguchi, K. Watanabe, N. Lu, S. K. Banerjee, K. L. Silverman, S. Kim, E. Tutuc, L. Yang, A. H. MacDonald, and X. Li, Evidence for moiré excitons in van der Waals heterostructures, *Nature* **567**, 71 (2019).
- [11] C. Jin, E. C. Regan, A. Yan, M. I. B. Utama, D. Wang, S. Zhao, Y. Qin, S. Yang, Z. Zheng, S. Shi, K. Watanabe, T. Taniguchi, S. Tongay, A. Zettl, and F. Wang, Observation of moiré excitons in WSe₂/WS₂ heterostructure superlattices, *Nature* **567**, 76 (2019).
- [12] P. Forn-Díaz, L. Lamata, E. Rico, J. Kono, and E. Solano, Ultrastrong coupling regimes of light-matter interaction, *Reviews of Modern Physics* **91** (2019).
- [13] A. F. Kockum, A. Miranowicz, S. D. Liberato, S. Savasta, and F. Nori, Ultrastrong coupling between light and matter, *Nature Reviews Physics* **1**, 19 (2019).
- [14] F. J. Garcia-Vidal, C. Ciuti, and T. W. Ebbesen, Manipulating matter by strong coupling to vacuum fields, *Science* **373** (2021).
- [15] F. Schlawin, D. M. Kennes, and M. A. Sentef, Cavity quantum materials, *Applied Physics Reviews* **9**, 011312 (2022).
- [16] J. Keller, G. Scalari, S. Cibella, C. Maissen, F. Appugliese, E. Giovine, R. Leoni, M. Beck, and J. Faist, Few-Electron Ultrastrong Light-Matter Coupling at 300 GHz with Nanogap Hybrid LC Microcavities, *Nano Letters* **17**, 7410 (2017).
- [17] G. Scalari, C. Maissen, D. Turcinkova, D. Hagemmüller, S. D. Liberato, C. Ciuti, C. Reichl, D. Schuh, W. Wegscheider, M. Beck, and J. Faist, Ultrastrong Coupling of the Cyclotron Transition of a 2D Electron Gas to a THz Metamaterial, *Science* **335**, 1323 (2012).
- [18] G. L. Paravicini-Bagliani, F. Appugliese, E. Richter, F. Valmorra, J. Keller, M. Beck, N. Bartolo, C. Rössler, T. Ihn, K. Ensslin, C. Ciuti, G. Scalari, and J. Faist, Magneto-transport controlled by Landau polariton states, *Nature Physics* **15**, 186 (2018).
- [19] F. Appugliese, J. Enkner, G. L. Paravicini-Bagliani, M. Beck, C. Reichl, W. Wegscheider, G. Scalari, C. Ciuti, and J. Faist, Breakdown of topological protection by cavity vacuum fields in the integer quantum Hall effect, *Science* **375**, 1030 (2022).
- [20] C. Ciuti, Cavity-mediated electron hopping in disordered quantum Hall systems, *Physical Review B* **104** (2021).
- [21] G. Arwas and C. Ciuti, Quantum electron transport controlled by cavity vacuum fields, *Physical Review B* **107** (2023).
- [22] O. Dmytruk and M. Schirò, Controlling topological phases of matter with quantum light, *Communications Physics* **5** (2022).

- [23] X. Wang, E. Ronca, and M. A. Sentef, Cavity quantum electrodynamical Chern insulator: Towards light-induced quantized anomalous Hall effect in graphene, *Physical Review B* **99** (2019).
- [24] J. Li, L. Schamriß, and M. Eckstein, Effective theory of lattice electrons strongly coupled to quantum electromagnetic fields, *Physical Review B* **105** (2022).
- [25] D. Guerci, P. Simon, and C. Mora, Superradiant Phase Transition in Electronic Systems and Emergent Topological Phases, *Phys. Rev. Lett.* **125**, 257604 (2020).
- [26] K. Masuki and Y. Ashida, Berry phase and topology in ultrastrongly coupled quantum light-matter systems, *Physical Review B* **107** (2023).
- [27] T. Karzig, C.-E. Bardyn, N. H. Lindner, and G. Refael, Topological Polaritons, *Phys. Rev. X* **5**, 031001 (2015).
- [28] T. Ozawa, H. M. Price, A. Amo, N. Goldman, M. Hafezi, L. Lu, M. C. Rechtsman, D. Schuster, J. Simon, O. Zilberberg, and I. Carusotto, Topological photonics, *Rev. Mod. Phys.* **91**, 015006 (2019).
- [29] F. Wu, T. Lovorn, E. Tutuc, I. Martin, and A. MacDonald, Topological Insulators in Twisted Transition Metal Dichalcogenide Homobilayers, *Physical Review Letters* **122** (2019).
- [30] D. Zhai and W. Yao, Theory of tunable flux lattices in the homobilayer moiré of twisted and uniformly strained transition metal dichalcogenides, *Physical Review Materials* **4** (2020).
- [31] See Supplementary Material for additional details about the cavity QED Hamiltonian, the purity of electronic reduced density matrix, the spectral functions and spatial distribution of edge states.
- [32] H. Yu, M. Chen, and W. Yao, Giant magnetic field from moiré induced Berry phase in homobilayer semiconductors, *National Science Review* **7**, 12 (2020).
- [33] R. Zhao, G.-D. Xie, M. L. N. Chen, Z. Lan, Z. Huang, and W. E. I. Sha, First-principle calculation of Chern number in gyrotropic photonic crystals, *Optics Express* **28**, 4638 (2020).
- [34] C. Cohen-Tannoudji, B. Diu, and F. Laloë, *Mécanique Quantique - Tome 1* (EDP Sciences, 2020).
- [35] R. Noguchi, M. Kobayashi, Z. Jiang, K. Kuroda, T. Takahashi, Z. Xu, D. Lee, M. Hirayama, M. Ochi, T. Shirasawa, P. Zhang, C. Lin, C. Bareille, S. Sakuragi, H. Tanaka, S. Kunisada, K. Kurokawa, K. Yaji, A. Harasawa, V. Kandyba, A. Giampietri, A. Barinov, T. K. Kim, C. Cacho, M. Hashimoto, D. Lu, S. Shin, R. Arita, K. Lai, T. Sasagawa, and T. Kondo, Evidence for a higher-order topological insulator in a three-dimensional material built from van der Waals stacking of bismuth-halide chains, *Nature Materials* **20**, 473 (2021).
- [36] C. Tao, L. Jiao, O. V. Yazyev, Y.-C. Chen, J. Feng, X. Zhang, R. B. Capaz, J. M. Tour, A. Zettl, S. G. Louie, H. Dai, and M. F. Crommie, Spatially resolving edge states of chiral graphene nanoribbons, *Nature Physics* **7**, 616 (2011).
- [37] M. E. Barber, E. Y. Ma, and Z.-X. Shen, Microwave impedance microscopy and its application to quantum materials, *Nature Reviews Physics* **4**, 61 (2021).
- [38] E. Prodan, T. L. Hughes, and B. A. Bernevig, Entanglement Spectrum of a Disordered Topological Chern Insulator, *Physical Review Letters* **105** (2010).
- [39] R. Bianco and R. Resta, Mapping topological order in coordinate space, *Physical Review B* **84** (2011).
- [40] Y.-F. Zhang, Y.-Y. Yang, Y. Ju, L. Sheng, R. Shen, D.-N. Sheng, and D.-Y. Xing, Coupling-matrix approach to the Chern number calculation in disordered systems, *Chinese Physics B* **22**, 117312 (2013).
- [41] M. D. Caio, G. Möller, N. R. Cooper, and M. J. Bhaseen, Topological marker currents in Chern insulators, *Nature Physics* **15**, 257 (2019).

Supplementary Material for the article:
“Electron-photon Chern number in cavity-embedded 2D moiré materials”

Danh-Phuong Nguyen,¹ Geva Arwas,¹ Zuzhang Lin,^{2,3} Wang Yao,^{2,3} and Cristiano Ciuti¹

¹*Université Paris Cité, CNRS, Matériaux et Phénomènes Quantiques, 75013 Paris, France*

²*Department of Physics, The University of Hong Kong, Hong Kong, China*

³*HKU-UCAS Joint Institute of Theoretical and Computational Physics at Hong Kong, China*
(Dated: September 27, 2023)

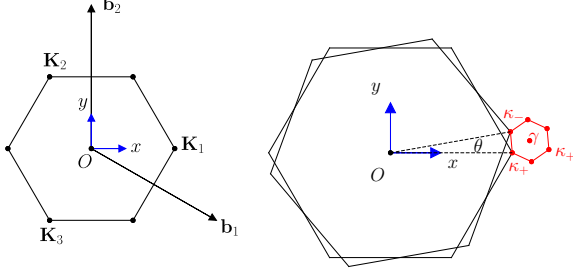


FIG. S1. First Brillouin zone with Dirac points of the bottom layer (left) and moiré Brillouin zone (shown in red) of moiré superlattice (right).

I. CAVITY QED HAMILTONIAN

In this section we derive a four-band continuum model^{1,2} for small angle twisted bilayer TMD. The electron-photon Hamiltonian can be written as:

$$\hat{H} = \hbar\omega_c \hat{a}^\dagger \hat{a} + \begin{pmatrix} \hat{H}_t & 0 \\ 0 & \hat{H}_b \end{pmatrix} + \begin{pmatrix} \hat{V}_t & \hat{U} \\ \hat{U}^\dagger & \hat{V}_b \end{pmatrix}, \quad (\text{S.1})$$

where \hat{a}^\dagger creates a photon of frequency ω_c , \hat{H}_t (\hat{H}_b) is a 2×2 matrix corresponding to the top (bottom) layer describing the TMD material along with the coupling to the cavity photon. The last term is a 4×4 matrix describing the moiré potential. \hat{V}_t and \hat{V}_b describe the intra-layer interactions, while \hat{U} is the layer-layer interaction. Each layer is a honeycomb lattice with the lattice constant a_0 and is defined by the two primitive vectors $\mathbf{a}_1 = a_0\sqrt{3}/2(1, \sqrt{3}, 0)$, $\mathbf{a}_2 = a_0\sqrt{3}/2(-1, \sqrt{3}, 0)$ and their reciprocal counterparts $\mathbf{b}_1 = 2\pi/(3a_0)(\sqrt{3}, 1, 0)$, $\mathbf{b}_2 = 2\pi/(3a_0)(-\sqrt{3}, 1, 0)$. The top layer is rotated in-plane by a small angle θ in order to create a moiré pattern. The mismatch between layers is given by $\Delta(\mathbf{r}) = [\mathbb{1} - R^{-1}(\theta)]\mathbf{r}$, where $R(\theta)$ is a rotation matrix about the z -axis. One moiré unit cell is defined by $\mathbf{L}_{i=1,2}$ such that $\Delta(\mathbf{L}_i) = \mathbf{a}_i$, hence $\mathbf{L}_i = [\mathbb{1} - R^{-1}(\theta)]^{-1}\mathbf{a}_i$. Similarly, the moiré reciprocal lattice vectors $\mathbf{G}_i = [\mathbb{1} - R(\theta)]\mathbf{b}_i$, satisfying $\mathbf{L}_i \cdot \mathbf{G}_j = 2\pi\delta_{ij}$.

Each layer is described by a tight binding Hamiltonian on the honeycomb lattice, with hopping coupling quantified by t . The unit cell consists of two sites A, B having an on-site energy difference of 2Δ . The electron-photon interaction is introduced via Peierls substitution. For the

bottom layer, we can write the Hamiltonian as:

$$\hat{H}_b = \Delta \sum_{\mathbf{R}} \left(|A, \mathbf{R}\rangle \langle A, \mathbf{R}| - |B, \mathbf{R}\rangle \langle B, \mathbf{R}| \right) + t \sum_{\mathbf{R}, j=1,2,3} e^{-ig(\hat{a} + \hat{a}^\dagger)\mathbf{u} \cdot \mathbf{e}_j} |B, \mathbf{R} + \mathbf{a}_j\rangle \langle A, \mathbf{R}| + \text{h.c.}, \quad (\text{S.2})$$

where $g = eA_0a_0/\hbar$, \mathbf{u} is the cavity orientation, $\mathbf{e}_{j=1,2,3} = R(j2\pi/3)(0, -1, 0)$ and $\mathbf{a}_3 = (0, 0, 0)$. We assume the cavity field \mathbf{A} is uniform, such that the Hamiltonian (S.2) is block-diagonal in \mathbf{k} space. The Bloch Hamiltonian $H_b^c(\mathbf{k})$ is given by:

$$\hat{H}_b^c(\mathbf{k}) = \Delta |A, \mathbf{k}\rangle \langle A, \mathbf{k}| - \Delta |B, \mathbf{k}\rangle \langle B, \mathbf{k}| + t \sum_{j=0,1,2} e^{-ig(\hat{a} + \hat{a}^\dagger)\mathbf{u} \cdot \mathbf{e}_j} e^{-i\mathbf{k} \cdot \mathbf{a}_j} |B, \mathbf{k}\rangle \langle A, \mathbf{k}| + \text{h.c.}, \quad (\text{S.3})$$

where \mathbf{k} is in the Brillouin zone (BZ) as shown in Figure S1. Next, we expand around one valley \mathbf{K}_b such that $\mathbf{K}_b \cdot \mathbf{a}_1 = -2\pi/3$, and at the first order in g , we have:

$$\hat{H}_b(\mathbf{k}) = \Delta\sigma_z + \frac{3a_0t}{2} \left(\mathbf{k} - \mathbf{K}_b + \frac{e\mathbf{A}^{(xy)}}{\hbar} (\hat{a} + \hat{a}^\dagger) \right) \cdot \boldsymbol{\sigma}, \quad (\text{S.4})$$

where $\boldsymbol{\sigma} = (\sigma_x, \sigma_y, \sigma_z)$ are the Pauli matrices for the sublattice degree of freedom, $\mathbf{A}^{(xy)}$ is the in-plane projection of the cavity field \mathbf{A} .

The top layer is rotated in real space by an angle θ such that the lattice vectors in equation (S.2) are transformed as $\mathbf{a} \rightarrow \tilde{\mathbf{a}} = R(\theta)\mathbf{a}$. Following the same procedure and restricting \mathbf{k} to the vicinity of $\mathbf{K}_t = R(\theta)\mathbf{K}_b$ one gets:

$$\hat{H}_t(\mathbf{k}) = \Delta\sigma_z + \frac{3a_0t}{2} R^{-1}(\theta) \left(\mathbf{k} - \mathbf{K}_t + \frac{e\mathbf{A}^{(xy)}}{\hbar} (\hat{a} + \hat{a}^\dagger) \right) \cdot \boldsymbol{\sigma}. \quad (\text{S.5})$$

In the presence of the cavity, the interlayer hopping \hat{U} between site \mathbf{R}_b of the bottom and \mathbf{R}_t of the top can be approximated as:

$$\hat{U} = \sum_{\substack{\mathbf{R}_b, \mathbf{R}_t \\ \sigma=A,B}} e^{-i\Phi_{\mathbf{R}_t, \mathbf{R}_b}(\hat{a} + \hat{a}^\dagger)} T(\mathbf{R}_t - \mathbf{R}_b) |\sigma, \mathbf{R}_t\rangle \langle \sigma, \mathbf{R}_b|, \quad (\text{S.6})$$

where $T(\mathbf{R}_t - \mathbf{R}_b)$ is the hopping coefficient in the absence of a cavity^{3,4}. We assume that the interlayer hopping is

only between sub-lattices of the same type. $\mathbf{R}_t - \mathbf{R}_b = \mathbf{d} + \mathbf{\Delta}(\mathbf{r})$ where $\mathbf{d} = d(0, 0, 1)$ is the distance between two layers. The Peierls phase can be approximated by $\Phi_{\mathbf{R}_t, \mathbf{R}_b} = e\mathbf{A} \cdot (\mathbf{R}_t - \mathbf{R}_b)/\hbar \approx eA^{(z)}d/\hbar$, where $A^{(z)}$ is the z -component of the cavity field. Since the Peierls phase does not depend on \mathbf{r} , we can write the interlayer coupling as:

$$\hat{U} = e^{-i\frac{eA^{(z)}d}{\hbar}(\hat{a} + \hat{a}^\dagger)} \hat{U}_0, \quad (\text{S.7})$$

where \hat{U}_0 is a moiré interlayer hopping in the absence of the cavity.

Combining all terms and defining $v_F = 3a_0t/(2\hbar)$ one gets a low-energy Hamiltonian for the twisted bilayer TMD coupled to cavity field:

$$\tilde{H} = \left(\begin{array}{c} \Delta\sigma_z + v_F R^{-1}(\theta) [\hat{\mathbf{p}} - \hbar\boldsymbol{\kappa}_- + e\mathbf{A}^{(xy)}(\hat{a} + \hat{a}^\dagger)] \cdot \boldsymbol{\sigma} + \hat{V}_t \\ e^{i\frac{eA^{(z)}d}{\hbar}(\hat{a} + \hat{a}^\dagger)} \hat{U}_0^\dagger \end{array} \quad \begin{array}{c} e^{-i\frac{eA^{(z)}d}{\hbar}(\hat{a} + \hat{a}^\dagger)} \hat{U}_0 \\ \Delta\sigma_z + v_F [\hat{\mathbf{p}} - \hbar\boldsymbol{\kappa}_+ + e\mathbf{A}^{(xy)}(\hat{a} + \hat{a}^\dagger)] \cdot \boldsymbol{\sigma} + \hat{V}_b \end{array} \right) + \hbar\omega_c \hat{a}^\dagger \hat{a}. \quad (\text{S.8})$$

Note that here we change the notation as \mathbf{K}_b (\mathbf{K}_t) $\rightarrow \boldsymbol{\kappa}_+$ ($\boldsymbol{\kappa}_-$) to highlight the moiré mini-BZ (see Fig. S1). Next, we apply the unitary transformation $\hat{T}_\theta = \text{diag}(e^{-i\frac{\theta}{2}\sigma_z}, \mathbb{1})$, leading to

$$\hat{T}_\theta \tilde{H} \hat{T}_\theta^\dagger = \left(\begin{array}{c} \Delta\sigma_z + v_F [\hat{\mathbf{p}} - \hbar\boldsymbol{\kappa}_- + e\mathbf{A}^{(xy)}(\hat{a} + \hat{a}^\dagger)] \cdot \boldsymbol{\sigma} + \hat{V}_t \\ e^{i\frac{eA^{(z)}d}{\hbar}(\hat{a} + \hat{a}^\dagger)} e^{i\frac{\theta}{2}\sigma_z} \hat{U}_0^\dagger \end{array} \quad \begin{array}{c} e^{-i\frac{eA^{(z)}d}{\hbar}(\hat{a} + \hat{a}^\dagger)} e^{-i\frac{\theta}{2}\sigma_z} \hat{U}_0 \\ \Delta\sigma_z + v_F [\hat{\mathbf{p}} - \hbar\boldsymbol{\kappa}_+ + e\mathbf{A}^{(xy)}(\hat{a} + \hat{a}^\dagger)] \cdot \boldsymbol{\sigma} + \hat{V}_b \end{array} \right) + \hbar\omega_c \hat{a}^\dagger \hat{a}. \quad (\text{S.9})$$

We remove the photonic operators from the off-diagonal terms using the unitary transformation $\hat{T}_d = \text{diag}(e^{i\frac{eA^{(z)}d}{2\hbar}(\hat{a} + \hat{a}^\dagger)}, e^{-i\frac{eA^{(z)}d}{2\hbar}(\hat{a} + \hat{a}^\dagger)})$. The photonic number operator transforms as $\hat{a}^\dagger \hat{a} \rightarrow \hat{a}^\dagger \hat{a} + i\frac{eA^{(z)}d}{2\hbar}(\hat{a} - \hat{a}^\dagger)\tau_z + \text{constant}$, where τ_z is the Pauli matrix with respect to the layer pseudo-spin. Finally, the four-band Hamiltonian $\hat{H}^{(4)} = \hat{T}_d \hat{T}_\theta \tilde{H} \hat{T}_\theta^\dagger \hat{T}_d^\dagger$ can be written as:

$$\hat{H}^{(4)} = \left(\begin{array}{c} \Delta\sigma_z + v_F [\hat{\mathbf{p}} - \hbar\boldsymbol{\kappa}_- + e\mathbf{A}^{(xy)}(\hat{a} + \hat{a}^\dagger)] \cdot \boldsymbol{\sigma} + \hat{V}_t \\ e^{i\frac{\theta}{2}\sigma_z} \hat{U}_0^\dagger \end{array} \quad \begin{array}{c} e^{-i\frac{\theta}{2}\sigma_z} \hat{U}_0 \\ \Delta\sigma_z + v_F [\hat{\mathbf{p}} - \hbar\boldsymbol{\kappa}_+ + e\mathbf{A}^{(xy)}(\hat{a} + \hat{a}^\dagger)] \cdot \boldsymbol{\sigma} + \hat{V}_b \end{array} \right) + \hbar\omega_c \hat{a}^\dagger \hat{a} + i\frac{\omega_c eA^{(z)}d}{2}(\hat{a} - \hat{a}^\dagger)\tau_z. \quad (\text{S.10})$$

II. EFFECTIVE MODEL FOR THE VALENCE BANDS

For the case of large Δ we can construct an effective model for the valence bands. Let $\Psi = (\Psi_t^c, \Psi_t^v, \Psi_b^c, \Psi_b^v)^T$

be an eigenvector of $\hat{H}^{(4)}$ with energy E , where c (v) corresponds to the conduction (valence) bands. Using (S.10), we can write

$$\begin{aligned} & (\Delta + \hat{V}_t^c + \hbar\omega_c \hat{a}^\dagger \hat{a} + \hat{D}) \Psi_t^c + v_F (\hat{\Pi}_{tx} - i\hat{\Pi}_{ty}) \Psi_t^v + e^{-i\frac{\theta}{2}} \hat{U}_0^c \Psi_b^c = E \Psi_t^c, \\ & v_F (\hat{\Pi}_{tx} + i\hat{\Pi}_{ty}) \Psi_t^c + (-\Delta + \hat{V}_t^v + \hbar\omega_c \hat{a}^\dagger \hat{a} + \hat{D}) \Psi_t^v + e^{i\frac{\theta}{2}} \hat{U}_0^v \Psi_b^v = E \Psi_t^v, \\ & (\Delta + \hat{V}_b^c + \hbar\omega_c \hat{a}^\dagger \hat{a} - \hat{D}) \Psi_b^c + v_F (\hat{\Pi}_{bx} - i\hat{\Pi}_{by}) \Psi_b^v + e^{i\frac{\theta}{2}} (\hat{U}_0^c)^\dagger \Psi_t^c = E \Psi_b^c, \\ & v_F (\hat{\Pi}_{bx} + i\hat{\Pi}_{by}) \Psi_b^c + (-\Delta + \hat{V}_b^v + \hbar\omega_c \hat{a}^\dagger \hat{a} - \hat{D}) \Psi_b^v + e^{-i\frac{\theta}{2}} (\hat{U}_0^v)^\dagger \Psi_t^v = E \Psi_b^v, \end{aligned} \quad (\text{S.11})$$

where for brevity we introduce the notation $\hat{\Pi}_{b,t} = \hat{\mathbf{p}} - \hbar\boldsymbol{\kappa}_{+,-} + e\mathbf{A}^{(xy)}(\hat{a} + \hat{a}^\dagger)$ and $\hat{D} = i\frac{\omega_c eA^{(z)}d}{2}(\hat{a} - \hat{a}^\dagger)$.

We consider a TMD material that has a large gap between the conduction and valence bands, and for

states localized in the latter, we have $E \approx -\Delta$ and $\|\Psi_t^c\|, \|\Psi_b^c\| \ll \|\Psi_t^v\|, \|\Psi_b^v\|$. Additionally, the moiré potentials and photon energy are also weak such that $\|\hat{U}_0\|, \|\hat{V}_t\|, \|\hat{V}_b\|, \hbar\omega_c \ll \Delta$. By neglecting higher order terms, the first two equations of (S.11) corresponding to

the top layer become:

$$\begin{aligned} 2\Delta\Psi_t^c + v_F \left(\hat{\Pi}_{tx} - i\hat{\Pi}_{ty} \right) \Psi_t^v &= 0, \\ v_F \left(\hat{\Pi}_{tx} + i\hat{\Pi}_{ty} \right) \Psi_t^c + \left(-\Delta + \hat{V}_t^v + \hbar\omega_c\hat{a}^\dagger\hat{a} - \hat{D} \right) \Psi_t^v + e^{i\frac{\theta}{2}}\hat{U}_0^v\Psi_b^v &= E\Psi_t^v. \end{aligned} \quad (\text{S.12})$$

Solving the first line for Ψ_t^c and defining the effective mass $m^* = \frac{\Delta}{v_F^2}$, the second line can be written as

$$\left(-\frac{[\hat{\mathbf{p}} - \hbar\boldsymbol{\kappa}_- + e\mathbf{A}^{(xy)}(\hat{a} + \hat{a}^\dagger)]^2}{2m^*} + \hat{V}_t^v - \Delta + \hbar\omega_c\hat{a}^\dagger\hat{a} + \hat{D} \right) \Psi_t^v + e^{i\frac{\theta}{2}}\hat{U}_0^v\Psi_b^v = E\Psi_t^v. \quad (\text{S.13})$$

Following the same procedure, we obtain another equation for the bottom layer with $\boldsymbol{\kappa}_- \rightarrow \boldsymbol{\kappa}_+$, $t \rightarrow b$. Combining the two equations we get an effective Hamiltonian for the valence bands:

$$\tilde{\mathcal{H}} = -\frac{1}{2m^*} \begin{pmatrix} (\hat{\mathbf{p}} - \hbar\boldsymbol{\kappa}_- + e\mathbf{A}^{(xy)}(\hat{a} + \hat{a}^\dagger))^2 & 0 \\ 0 & (\hat{\mathbf{p}} - \hbar\boldsymbol{\kappa}_+ + e\mathbf{A}^{(xy)}(\hat{a} + \hat{a}^\dagger))^2 \end{pmatrix} + \begin{pmatrix} \hat{V}_t^v & \hat{U}_0^v \\ \hat{U}_0^{v\dagger} & \hat{V}_b^v \end{pmatrix} + \hbar\omega_c\hat{a}^\dagger\hat{a} + i\omega_c\frac{eA^{(z)}d}{2}(\hat{a} - \hat{a}^\dagger)\tau_z. \quad (\text{S.14})$$

The intralayer moiré potentials \hat{V}_t^v and \hat{V}_b^v can be written as^{1,2}:

$$V_{t/b}^v(\mathbf{r}) = V_0 \sum_{i=1}^3 \cos(\mathbf{K}_i \cdot \boldsymbol{\Delta}(\mathbf{r}) \pm \alpha), \quad (\text{S.15})$$

where \mathbf{K}_i are shown in Fig. S1. In order to simplify the calculation, one could use the relation $\mathbf{K}_i \cdot \boldsymbol{\Delta}(\mathbf{r}) = \mathbf{G}_i \cdot \mathbf{r}$, where $\mathbf{G}_{1,2}$ are reciprocal lattice vectors of the moiré system defined above and $\mathbf{G}_3 = \mathbf{G}_1 - \mathbf{G}_2$. The interlayer coupling \hat{U}_0^v is given by^{1,2}:

$$U_0^v(\mathbf{r}) = h_0 \sum_{j=1}^3 e^{i(\mathbf{G}_j - \mathbf{G}_1) \cdot \mathbf{r}}. \quad (\text{S.16})$$

For the numerical simulations presented in the paper we used the parameters of MoTe₂: $m^* \approx 0.62m_e$ where m_e is the bare electron mass, $a_0 \approx 3.5\text{\AA}$, $d \approx 10\text{\AA}$, moiré potentials $(V_0, \alpha, h_0) \approx (16 \text{ meV}, 89.6^\circ, -8.5 \text{ meV})^1$.

III. PARTICLE-HOLE TRANSFORMATION

In this section we detail the present model (S.14) in the hole picture. In second quantization, (S.14) reads:

$$\begin{aligned} \tilde{\mathcal{H}} &= \hbar\omega_c\hat{a}^\dagger\hat{a} - \frac{\hbar^2}{2m^*} \sum_{\mathbf{q},\nu} \hat{c}_{\nu\mathbf{q}}^\dagger \left[\mathbf{q} - \mathbf{K}_\nu + \frac{e\mathbf{A}^{(xy)}}{\hbar}(\hat{a} + \hat{a}^\dagger) \right]^2 \hat{c}_{\nu\mathbf{q}} + \sum_\nu \int d\mathbf{r} \hat{c}_{\nu}^\dagger(\mathbf{r}) V_\nu^v(\mathbf{r}) \hat{c}_\nu(\mathbf{r}) \\ &+ \int d\mathbf{r} \left[\hat{c}_t^\dagger(\mathbf{r}) U_0^v(\mathbf{r}) \hat{c}_b(\mathbf{r}) + \text{h.c.} \right] + i\omega_c \frac{eA^{(z)}d}{2} (\hat{a} - \hat{a}^\dagger) \int d\mathbf{r} \left(\hat{c}_t^\dagger(\mathbf{r}) \hat{c}_t(\mathbf{r}) - \hat{c}_b^\dagger(\mathbf{r}) \hat{c}_b(\mathbf{r}) \right), \end{aligned} \quad (\text{S.17})$$

where $\nu = t, b$ and $\mathbf{K}_{b,t} = \boldsymbol{\kappa}_{+,-}$. The particle-hole transformation can be defined by a unitary operator $\hat{\Gamma}$, such that $\hat{\Gamma}\hat{c}_\nu^\dagger(\mathbf{r})\hat{\Gamma}^\dagger = \hat{c}_\nu(\mathbf{r})$. Under this transformation the momentum operators transform as $\hat{c}_{\nu\mathbf{q}}^\dagger \rightarrow \hat{\Gamma}\hat{c}_{\nu\mathbf{q}}^\dagger\hat{\Gamma}^\dagger = \hat{c}_{\nu-\mathbf{q}}$. Using the particle-hole transformation, the Hamiltonian $\hat{\mathcal{H}} = \hat{\Gamma}\tilde{\mathcal{H}}\hat{\Gamma}^\dagger$ becomes:

$$\begin{aligned} \hat{\mathcal{H}} &= \hbar\omega_c\hat{a}^\dagger\hat{a} + \frac{\hbar^2}{2m^*} \sum_{\mathbf{q},\nu} \hat{c}_{\nu\mathbf{q}}^\dagger \left[\mathbf{q} + \mathbf{K}_\nu - \frac{e\mathbf{A}^{(xy)}}{\hbar}(\hat{a} + \hat{a}^\dagger) \right]^2 \hat{c}_{\nu\mathbf{q}} - \sum_\nu \int d\mathbf{r} \hat{c}_{\nu}^\dagger(\mathbf{r}) V_\nu^v(\mathbf{r}) \hat{c}_\nu(\mathbf{r}) \\ &- \int d\mathbf{r} \left[\hat{c}_b^\dagger(\mathbf{r}) U_0^v(\mathbf{r}) \hat{c}_t(\mathbf{r}) + \text{h.c.} \right] - i\omega_c \frac{eA^{(z)}d}{2} (\hat{a} - \hat{a}^\dagger) \int d\mathbf{r} \left(\hat{c}_t^\dagger(\mathbf{r}) \hat{c}_t(\mathbf{r}) - \hat{c}_b^\dagger(\mathbf{r}) \hat{c}_b(\mathbf{r}) \right). \end{aligned} \quad (\text{S.18})$$

Equation (S.18) results in the change of the sign of the effective mass, the charge and the moiré potentials. Note

that we have disregarded divergent sums that result from the interaction of all valence electrons with the photonic field. This is justified if we assume the light-matter interaction vanishes when all valence mini-bands are completely filled.

IV. PURITY OF MIXED STATES

We provide here more details about the purity of the electronic reduced density matrix that is discussed in the manuscript. By diagonalizing the light-matter Hamiltonian in Equation (3) in the main text, one obtains electron-photon eigenstates $|\Psi^{(e-p)}\rangle$ that belong to the Hilbert space, which is the product of the electron and photon Hilbert spaces. If one wants to focus on the electronic properties only, the standard approach is to consider the reduced density matrix defined as⁵ $\hat{\rho} = \text{Tr}_{\text{phot}}(|\Psi^{(e-p)}\rangle\langle\Psi^{(e-p)}|)$, where the trace is here over the photonic degrees of freedom. The purity of a density matrix is defined as $\mathbb{P} = \text{Tr}_{\text{el}}(\hat{\rho}^2)$, where here the trace is over the electronic degrees of freedom. Indeed, when the reduced density matrix describes a pure state, the purity is equal to 1, since $\hat{\rho}^2 = \hat{\rho}$ in that case. This occurs for electron-photon states that are separable, namely of the form $|\Psi^{(e-p)}\rangle = |\psi^{(e)}\rangle \otimes |\phi^{(p)}\rangle$, implying that the purity is merely $\text{Tr}_{\text{el}}(\hat{\rho}^2) = \text{Tr}_{\text{el}}(\hat{\rho}) = \text{Tr}_{\text{el}}(|\psi^{(e)}\rangle\langle\psi^{(e)}|) = 1$. Instead, when the reduced density matrix is mixed, it can be written as $\hat{\rho} = \sum_{\lambda=1}^d p_{\lambda} |\psi_{\lambda}^{(e)}\rangle\langle\psi_{\lambda}^{(e)}|$ where $\{|\psi_{\lambda}^{(e)}\rangle\}$ is an orthonormal basis of an electronic Hilbert subspace of dimension d and p_{λ} is the probability of finding the state in $|\psi_{\lambda}^{(e)}\rangle$, with $0 \leq p_{\lambda} \leq 1$ and $\sum_{\lambda=1}^d p_{\lambda} = 1$. These conditions lead to $\text{Tr}_{\text{el}}(\hat{\rho}^2) = \sum_{\lambda} p_{\lambda}^2 \leq \sum_{\lambda} p_{\lambda} = 1$. Moreover, the Cauchy-Schwarz inequality gives $\sum_{\lambda} p_{\lambda}^2 \geq 1/d$: hence, the purity reaches its minimum value $1/d$ if and only if $\forall \lambda, p_{\lambda} = 1/d$, which is known as a maximally mixed state. When the dimension d tends to infinity, the purity tends to 0.

V. EFFECTIVE ELECTRONIC HAMILTONIAN IN HIGH PURITY REGIME

In this section, we provide details about the effective electronic Hamiltonian obtained by adiabatic elimination of the photonic degree of freedom^{6,7}. Moreover, we use this theory to compare to the topological diagram in Fig. 2 of the main text, where the electron purity is very close to 1. Fig. 2 in the manuscript has been calculated using the exact electron-photon eigenstates and the electron-photon Chern number. The topological phase boundary in Fig. 2 can be calculated approximately by using the eigenstates of the effective electronic Hamiltonian and the traditional electron Chern number. Such approach works well in the regime considered in Fig. 2, where the electronic purity is close to 1.

Let us see here the details of the effective electronic Hamiltonian. Eq. (3) in main text can be written as $\hat{\mathcal{H}} =$

$\hat{\mathcal{H}}_0 + \hbar\omega_c \hat{a}^\dagger \hat{a} + D(\hat{a} + \hat{a}^\dagger)^2 + \hat{V}_{xy}(\hat{a} + \hat{a}^\dagger) + \hat{V}_z i(\hat{a} - \hat{a}^\dagger)$, where $\hat{\mathcal{H}}_0$ is the bare electronic Hamiltonian with its eigenstates $|\psi_{n\mathbf{k}}^0\rangle$ and energies $\epsilon_{n\mathbf{k}}^0$. The term $D = e^2 |\mathbf{A}^{(xy)}|^2 / (2m^*)$ is due to the diamagnetic energy, while \hat{V}_{xy} and \hat{V}_z are respectively in-plane and out-of-plane coupling term with the following form:

$$\hat{V}_{xy} = -\frac{e}{m^*} \mathbf{A}^{(xy)} \cdot \begin{pmatrix} \hat{\mathbf{p}} + \hbar\boldsymbol{\kappa}_- & 0 \\ 0 & \hat{\mathbf{p}} + \hbar\boldsymbol{\kappa}_- \end{pmatrix}, \quad (\text{S.19})$$

$$\hat{V}_z = \frac{\omega_c e A^{(z)} d}{2} \begin{pmatrix} 1 & 0 \\ 0 & -1 \end{pmatrix}.$$

By performing a Bogoliubov transformation for the photonic degrees of freedom, we can diagonalize the photonic part in the form $\hbar\omega_c \hat{a}^\dagger \hat{a} + D(\hat{a} + \hat{a}^\dagger)^2 = \hbar\tilde{\omega}_c \hat{\alpha}^\dagger \hat{\alpha}$, where the dressed photon frequency reads $\tilde{\omega}_c = \sqrt{\omega_c^2 + 2\omega_c e^2 |\mathbf{A}^{(xy)}|^2 / (m^* \hbar)}$ and the corresponding dressed boson operators are such that: $\hat{a} + \hat{a}^\dagger = \sqrt{\omega_c / \tilde{\omega}_c} (\hat{\alpha} + \hat{\alpha}^\dagger)$ and $\hat{a} - \hat{a}^\dagger = \sqrt{\tilde{\omega}_c / \omega_c} (\hat{\alpha} - \hat{\alpha}^\dagger)$. At the lowest order in perturbation theory, there is an effective coupling between different miniband states via an intermediate state with a (dressed) cavity photon. Namely, we have

$$|\psi_{n\mathbf{k}}^0\rangle|0\rangle \rightarrow |\psi_{\lambda\mathbf{k}}^0\rangle|1\rangle \rightarrow |\psi_{n'\mathbf{k}}^0\rangle|0\rangle. \quad (\text{S.20})$$

Such a process couples $|\psi_{n\mathbf{k}}^0\rangle$ and $|\psi_{n'\mathbf{k}}^0\rangle$ with a corresponding coupling energy:

$$\Gamma_{n'n\mathbf{k}} \simeq \frac{1}{2} \sum_{\lambda\mathbf{k}} \left(\frac{V_{n'\lambda\mathbf{k}} V_{\lambda n\mathbf{k}}}{\epsilon_{\lambda\mathbf{k}}^0 + \hbar\tilde{\omega}_c - \epsilon_{n'\mathbf{k}}^0} + \frac{V_{n'\lambda\mathbf{k}} V_{\lambda n\mathbf{k}}}{\epsilon_{\lambda\mathbf{k}}^0 + \hbar\tilde{\omega}_c - \epsilon_{n\mathbf{k}}^0} \right), \quad (\text{S.21})$$

with $V_{n'n\mathbf{k}} = \langle\psi_{n'\mathbf{k}}^0|\beta\hat{V}_{xy} + \beta^{-1}\hat{V}_z|\psi_{n\mathbf{k}}^0\rangle$ and $\beta = \sqrt{\omega_c / \tilde{\omega}_c}$. The effective electronic Hamiltonian reads:

$$\hat{\mathcal{H}}_{\text{eff}} = \sum_{n,\mathbf{k}} \epsilon_{n\mathbf{k}}^0 |\psi_{n\mathbf{k}}^0\rangle\langle\psi_{n\mathbf{k}}^0| + \sum_{n',n,\mathbf{k}} \Gamma_{n'n\mathbf{k}} |\psi_{n'\mathbf{k}}^0\rangle\langle\psi_{n\mathbf{k}}^0|. \quad (\text{S.22})$$

Equations (S.21) and (S.22) are valid only when the photon can be adiabatically eliminated. The agreement in Fig. 2 of the main text is excellent with only small variations at larger couplings due to the small deviations of the electron purity from unity with the parameters considered there.

VI. ELECTRONIC SPECTRAL FUNCTION AND SPATIAL DISTRIBUTION

In this section, we provide some details about the electron spectral function, a quantity that can be measured via Angular Resolved Photo-Emission Spectroscopy (ARPES) and the spatial distribution of the edge states, which can be measured for example via Scanning Tunneling Microscopy (STM) or Microwave Impedance Microscopy. In this section, we will consider ribbon samples with open boundary conditions in the short direction. The spatially resolved electronic density of state is given by:

$$A(\mathbf{k}, \omega, r_1) = \sum_n \sum_{\nu=t,b} \int dr_2 \left| \langle \Psi_{n\mathbf{k}}^{(e-p)} | r_1, r_2, \nu, \mathbf{k}, 0 \rangle \right|^2 \delta(\omega - \mathcal{E}_{n\mathbf{k}}^{(e-p)}), \quad (\text{S.23})$$

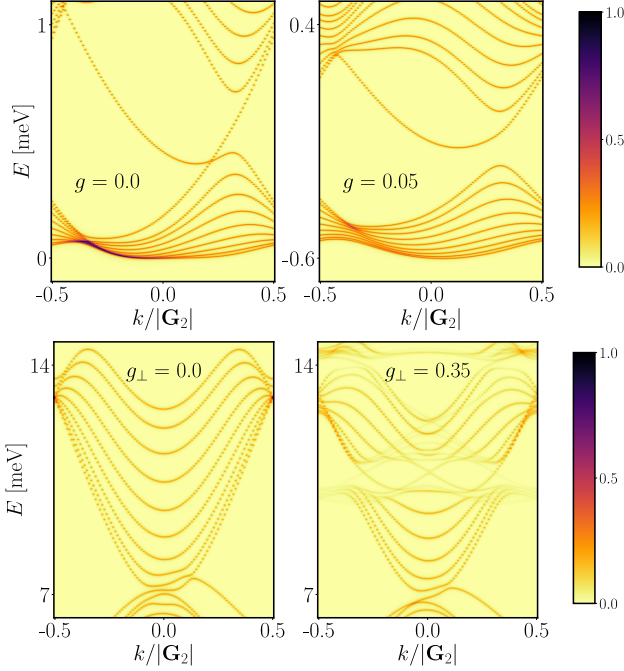


FIG. S2. Color plot of the electron spectral function (amplitude normalized by its maximum value) corresponding to the off-resonant (top panels) and resonant (bottom panels) configurations considered in Fig. 3 and 5 of the manuscript, respectively.

where r_1 (r_2) corresponds to the position in the short (long) direction, $\nu = t, b$ describes the layer degree of freedom. Moreover, $|\Psi_{n\mathbf{k}}^{(e-p)}\rangle$ and $\mathcal{E}_{n\mathbf{k}}^{(e-p)}$ are respectively electron-photon eigenstates and energies of the Hamiltonian, while $|0\rangle$ is a zero-photon state. Note that the domain of r_2 is restricted to one unit cell. From (S.23), the spectral function is directly obtained by taking the integral $\int dr_1$ of the spectral function A . Detailed plots of this observable are reported in Fig. S2, which has the same parameters as in Fig. 3 and 5 of the manuscript.

Given an electron-photon eigenstate $|\Psi_{n\mathbf{k}}^{(e-p)}\rangle$, its spatial distribution on the short direction (open boundary) is calculated by tracing over all the other degrees of freedom, namely:

$$\mathcal{D}_{n\mathbf{k}}^{(e-p)}(r_1) = \text{Tr}_{\text{phot}, r_2, \nu} \left(|\Psi_{n\mathbf{k}}^{(e-p)}\rangle \langle \Psi_{n\mathbf{k}}^{(e-p)}| \right). \quad (\text{S.24})$$

However, equation (S.24) is not the electronic local density of states. Instead from (S.23) the electronic local density of states is calculated as:

$$\begin{aligned} D_{n\mathbf{k}}^{(e)}(r_1) &= \int_{\mathcal{E}_{n\mathbf{k}}^{(e-p)} - \Delta\mathcal{E}}^{\mathcal{E}_{n\mathbf{k}}^{(e-p)} + \Delta\mathcal{E}} d\omega A(\mathbf{k}, \omega, r_1) \\ &\simeq \sum_{\nu=t,b} \int dr_2 \left| \langle \Psi_{n\mathbf{k}}^{(e-p)} | r_1, r_2, \nu, \mathbf{k}, 0 \rangle \right|^2. \end{aligned} \quad (\text{S.25})$$

The spatial distribution of the edge states created by the cavity coupling is reported in Fig. S3.

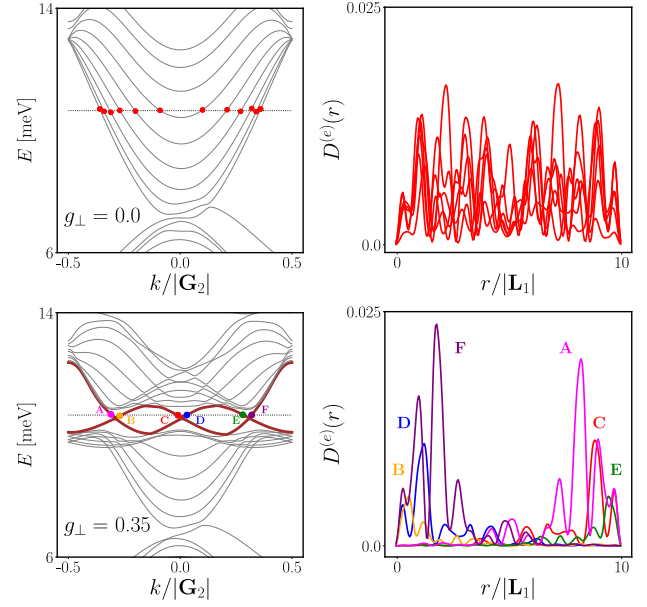


FIG. S3. Spatial distribution of the states indicated in the energy-momentum diagram for the electron-photon eigenstates. The top panels correspond to no cavity coupling, while the bottom panels correspond to the same configuration (perpendicular polarization) and parameters as in Fig. 5 of the manuscript.

[1] Fengcheng Wu, Timothy Lovorn, Emanuel Tutuc, Ivar Martin, and A. H. MacDonald, “Topological Insulators in Twisted Transition Metal Dichalcogenide Homobilayers,”

Physical Review Letters **122** (2019).

[2] Dawei Zhai and Wang Yao, “Theory of tunable flux lattices in the homobilayer moiré of twisted and uniformly

- strained transition metal dichalcogenides,” *Physical Review Materials* **4** (2020).
- [3] Yong Wang, Zhan Wang, Wang Yao, Gui-Bin Liu, and Hongyi Yu, “Interlayer coupling in commensurate and incommensurate bilayer structures of transition-metal dichalcogenides,” *Physical Review B* **95** (2017).
- [4] Rafi Bistritzer and Allan H. MacDonald, “Moiré bands in twisted double-layer graphene,” *Proceedings of the National Academy of Sciences* **108**, 12233–12237 (2011).
- [5] Claude Cohen-Tannoudji, Bernard Diu, and Franck Laloë, *Mécanique Quantique - Tome 1* (EDP Sciences, 2020).
- [6] Cristiano Ciuti, “Cavity-mediated electron hopping in disordered quantum Hall systems,” *Physical Review B* **104** (2021).
- [7] Geva Arwas and Cristiano Ciuti, “Quantum electron transport controlled by cavity vacuum fields,” *Physical Review B* **107** (2023).